Functionalized Squaraine Donors for Nanocrystalline Organic Photovoltaics

Guodan Wei,[†] Xin Xiao,[‡] Siyi Wang,[§] Kai Sun,[†] Kevin J. Bergemann,[⊥] Mark E. Thompson,[§] and Stephen R. Forrest[†,‡,⊥,*]

[†]Department of Materials Science and Engineering, University of Michigan, Ann Arbor, Michigan 48109, United States , [‡]Department of Electrical Engineering and Computer Science, University of Michigan, Ann Arbor, Michigan 48109, United States , [§]Department of Chemistry, University of Southern California, Los Angeles, California 90089, United States , and [⊥]Department of Physics, University of Michigan, Ann Arbor, Michigan 48109, United States

ABSTRACT

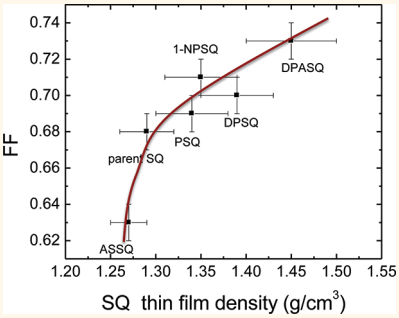

We study a family of functionalized squaraine (*f*SQ) donors for absorbing in the near-infrared (NIR) and green spectral regions. The NIR-absorbing materials are the symmetric molecules 2,4-bis[4-(*N*-phenyl-1-naphthylamino)-2,6-dihydroxyphenyl]squaraine (1-NPSQ), 2,4-bis[4-(*N*,*N*-diphenylamino)-2,6 dihydroxyphenyl]squaraine, and 2,4-bis[4-(*N*,*N*-dipropylamino)-2,6-dihydroxyphenyl]squaraine. The green light absorbing donors are asymmetric squaraines, namely, 2,4-bis[4-(*N*,*N*-diphenylamino)-2,6-dihydroxyphenyl]squaraine and 2-[4-(*N*,*N*-diisobutylamino)-2,6-dihydroxyphenyl]-4-diphenylamino]squaraine. Substitution of the arylamine groups enhances intermolecular packing, thereby increasing hole transport and the possibility of forming extended nanocrystalline junctions when annealed. Nanocrystalline solar cells based on *f*SQ and a C_{60} acceptor have $V_{oc} = 1.0$ V and fill factors 0.73 ± 0.01. Solar cells incorporating annealed 1-NPSQ films result in a power conversion efficiency of $5.7 \pm 0.6\%$ at 1 sun, AM1.5G illumination.

KEYWORDS: solution process · small molecule · solar cell

To improve the performance of bulk heterojunction (BHJ) polymeric solar cells, research has focused on controlling donor/acceptor phase separation (and hence interface area) and crystallinity[1] that leads to increased efficiency for exciton dissociation and conductivity.[2,3] Nanocrystalline HJs (ncHJ) in small-molecule organic solar cells with active layers deposited by vapor deposition[4,5] lead to an analogous, high interfacial surface area and crystallinity. Furthermore, when soluble molecules are blended in the liquid phase with fullerene-based acceptors, ordered molecular stacking is disrupted, forming isolated islands[6] that inhibit the formation of low-resistance, percolating transport paths for carriers.[7,8] However, solvent[9] or thermal annealing[10,11] can improve donor/acceptor phase separation in blends while also improving charge transport. In particular, we have explored ncHJs consisting of squaraine-based donors combined with a C_{60} acceptor.[10] This process has resulted in both a high fill factor (FF $\approx$ 0.7) and power conversion efficiency of $\eta_p \approx 6\%$.

Due to the facile synthetic paths to functionalizing squaraine dyes, these highly absorptive and stable materials have been extensively investigated from both fundamental and technological viewpoints.[12,13] In this work, we incorporate a family of functionalized squaraines (*f*SQ) in ncHJ structures to investigate correlations between molecular structure, film morphology, and device properties. For this study, based on the parent squaraine (SQ) 2,4-bis[4-(*N*,*N*-diisobutylamino)-2,6-dihydroxyphenyl]squaraine, we synthesize three symmetric donors, namely, 2,4-bis[4-(*N*-phenyl-1-naphthylamino)-2,6-dihydroxyphenyl]squaraine (1-NPSQ), 2,4-bis[4-(*N*,*N*-diphenylamino)-2,6 dihydroxyphenyl]squaraine (DPSQ), and 2,4-bis[4-(*N*,*N*-dipropylamino)-2,6-dihydroxyphenyl]squaraine (PSQ), along with two asymmetric squaraine donors, 2,4-bis[4-(*N*,*N*-diphenylamino)-2,6-dihydroxyphenyl]squaraine (DPASQ) and 2-[4-(*N*,*N*-diisobutylamino)-2,6-dihydroxyphenyl]-4-diphenylamino]squaraine (ASSQ). The molecular structural formulas of all these compounds are shown in Figure 1. Here N-aryl (in 1-NPSQ, DPSQ, DPASQ, and ASSQ) and N-propyl groups (in PSQ) are substituted for the alkylamines in the parent SQ.[14] The butyl end-groups of the parent SQ sterically limit its close packing of adjacent molecules, which in turn limits its hole conductivity and exciton diffusion length (L_D) (Table 1). Replacement of the end-groups with planar

* Address correspondence to stevefor@umich.edu.

Received for review December 1, 2011 and accepted December 23, 2011.

Published online December 23, 2011
10.1021/nn204676j

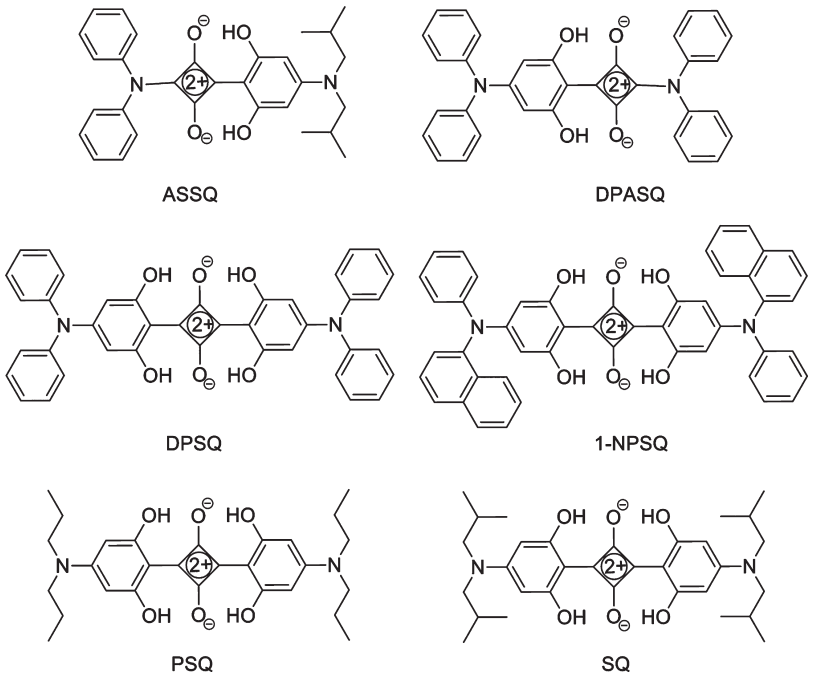

Figure 1. Molecular structural formulas of the functionalized squaraine donors.

TABLE 1. Physical Properties of Squaraine Donors

molecular species	HOMO (eV)	E_{opt} (eV)	ρ (g/cm^3)	L_D (nm)
DPASQ	5.4	1.9	1.45 ± 0.05	10.7 ± 0.2
DPSQ	5.3	1.5	1.39 ± 0.04	3.4 ± 0.7
PSQ	5.2	1.5	1.34 ± 0.04	NA
1-NPSQ	5.3	1.6	1.35 ± 0.04	2.9 ± 0.8
SQ	5.1	1.6	1.29 ± 0.03	1.6 ± 0.2
ASSQ	5.3	2.1	1.27 ± 0.02	11.0 ± 0.6

aryl moieties exerts control over the crystalline morphology by influencing the intermolecular contact distance while tuning the optical absorption spectrum and energy levels of the films. We find that annealed 1-NPSQ/C_{60} ncHJ solar cells have $V_{oc} = 0.90 \pm 0.01$, FF = 0.64 ± 0.01, and $J_{sc} = 10.0 \pm 1.1$ mA/cm^2 due to the combination of a deep, highest occupied molecular orbital (HOMO) energy (and hence high open circuit voltage, V_{oc}) and significant solar spectral coverage along with a high hole conductivity that results in a high short-circuit current (J_{sc}). For optimized and annealed 1-NPSQ/C_{60} cells, $\eta_p = 5.7 \pm 0.6\%$.[15]

RESULTS

The *f*SQs have lower HOMO energies than that of SQ, as shown in Table 1. Here, PSQ contains propyl amines, similar to isobutyl amines in SQ, resulting in a HOMO that is lower than that of SQ by 0.1 eV. All the other *f*SQs with aryl amines have even deeper HOMOs of 5.3 eV (1-NPSQ, DPSQ, and ASSQ) and 5.4 eV (DPASQ). In combination with the C_{60} acceptor, the interface offset provides sufficient energy for efficient exciton dissociation.

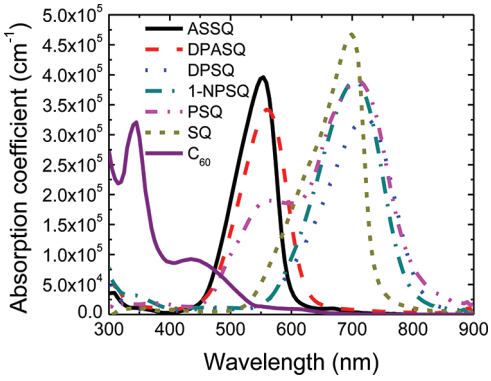

Figure 2. Absorption spectra of ASSQ, DPASQ, DPSQ, 1-NPSQ, PSQ, SQ, and C_{60}.

The absorption spectra of the *f*SQ films are shown in Figure 2. They exhibit a narrow and intense absorption band with maxima at wavelengths of $\lambda = 554, 560, 700, 710, 710$, and 720 nm, with corresponding peak absorption coefficients of 4.0, 3.4, 4.6, 4.0, 4.0, and 3.5 × 10^5 cm^{-1} for ASSQ, DPASQ, SQ, 1-NPSQ, PSQ, and DPSQ, respectively. PSQ has the broadest absorption, with a full width at half-maximum of $\Delta\lambda = 210$ nm (5100 cm^{-1}) and two peaks apparent in the spectrum.

The external quantum efficiencies (EQE) of the *f*SQ/C_{60} OPV cells are shown in Figure 3a. The peak EQE = 30% is due to the SQ absorption, whereas the peak efficiencies of 26% and 40% centered at λ= 350 and 470 nm result from C_{60} absorption. The PSQ devices have the highest peak EQE (41%) for C_{60}, with the EQE of PSQ, reaching 33% at λ = 710 nm. The other two symmetric cells, 1-NPSQ/C_{60} and DPSQ/C_{60}, have comparable C_{60} peak efficiencies of EQE = 32% at

λ= 470 nm and 25% at λ = 350 nm. Also, DPSQ has a red-shifted EQE response from the SQ peak. The ASSQ/C_{60} devices have a C_{60} response similar to the SQ/C_{60} cells. The DPASQ/C_{60} cells have lower EQE responses compared with ASSQ/C_{60} cells, consistent with the lower absorption efficiency of DPASQ, as shown in Figure 2. The EQE is ultimately limited by the trade-off between the absorption coefficient and the necessity to employ thin films due to the relatively short exciton diffusion lengths in the *f*SQs. The other material properties and cell performances for this family of donors are listed in Tables 1 and 2.

The *J*–*V* characteristics of the *f*SQs/C_{60} OPV cells at 1 sun illumination are shown in Figure 3b, with details listed in Table 2. Here, V_{oc} = 0.90 ± 0.01 V is observed for 1-NPSQ, DPSQ, and ASSQ and 1.0 ± 0.01 V for DPASQ, which is consistent with the increased interface energy difference, ΔE_{HL}, between HOMOs of the donors and the LUMO of C_{60}[16] (where ΔE_{HL} = 1.3 to 1.4 eV) compared with ΔE_{HL} = 1.1 eV for SQ/C_{60}. Moreover, DPASQ/C_{60} devices have the highest FF = 0.73 ± 0.01 at 1 sun. However, the blue-shifted absorption of DPASQ limits the J_{sc}. In contrast, PSQ/C_{60} cells have J_{sc} = 9.5 ± 0.1 mA/cm^2, which is consistent with the high EQE in Figure 3a. The relatively broad absorption of PSQ improves photon harvesting throughout the wavelength range from λ = 550 to 850 nm.

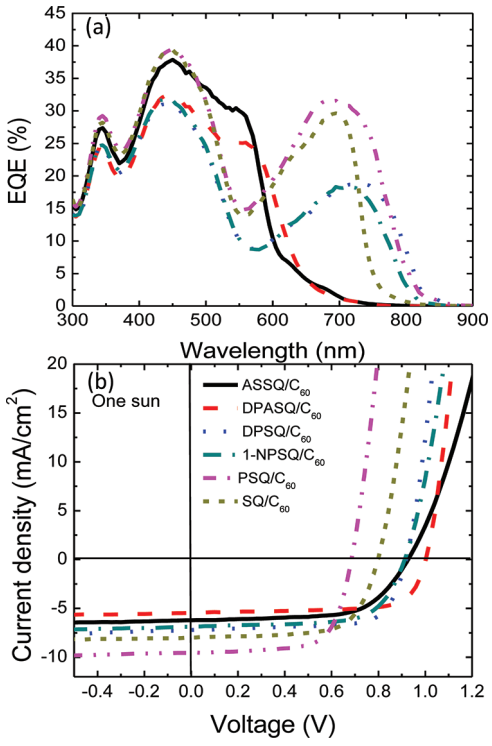

Figure 3. (a) External quantum efficiencies (EQE) and (b) current density (*J*) *versus* voltage (*V*) characteristics at 1 sun illumination of the six as-cast *f*SQ/C_{60} cells with the structure ITO/MoO_3(80 Å)/SQs(85 ± 5 Å)/C_{60}(400 Å)/3,4,9,10-perylene-tetracarboxylic bisbenzimidazole (PTCBI) (80 Å)/Ag (1000 Å).

The FF *versus* incident power intensity is shown in Figure 4a. Here, FF of the DPASQ/C_{60} cells reaches 0.77 ± 0.01 at low intensity, gradually decreasing to 0.73 ± 0.01 at 1 sun. The DPSQ/C_{60} cells have FF ranging from 0.70 ± 0.01 to 0.74 ± 0.01 throughout the measured power intensities. The other symmetric squaraine donor cells (1-NPSQ, PSQ, and SQ) have relatively high and intensity-independent FF (>0.66) as well. In contrast, the FF of the ASSQ/C_{60} cells falls off sharply, from 0.70 ± 0.01 at 0.002 suns to 0.56 ± 0.01 at 1.7 suns.

The power conversion efficiency, η_p, as a function of incident power intensity is shown in Figure 4b. Consistent with their high FF, the power efficiency of the DPSQ/C_{60} cell increases from η_p = 3.4 ± 0.2% at low intensity to 4.8 ± 0.2% at 1 sun. With the exception of the ASSQ/C_{60} cells, the efficiency of the remaining five *f*SQ-based OPV cells increases with power intensity, which differs from roll-off in η_p previously reported for SQ/fullerene solar cells.[6] The roll-off in η_p of ASSQ/C_{60} cells is due to the decrease in FF, as shown in Figure 4a.

DISCUSSION

The AFM images of thin films cast on 80 Å thick MoO_3 buffer layers shown in Figure 5 suggest a variation in surface morphologies for different *f*SQs. The films in Figure 5 have root-means-square (rms) roughnesses of 8.8 ± 2.0, 5.8 ± 1.0, 1.4 ± 0.5, 1.2 ± 0.6, 0.9 ± 0.2, and 0.6 ± 0.2 nm for nanocrystalline PSQ and amorphous DPSQ, ASSQ, 1-NPSQ, SQ, and DPASQ, respectively. The nanocrystalline morphology of PSQ creates a high density of protrusions, ultimately resulting in an increased interface area with the subsequently deposited C_{60}. This promotes improved exciton dissociation, generating holes that are readily transported to the anode, which, in turn, results in an increased peak EQE = 41% for light absorbed in the C_{60}. In combination

TABLE 2. Performance of As-Cast *f*SQ/C_{60} Solar Cells under 1 sun, AM1.5G Simulated Illumination and in the Dark

molecular species	V_{oc} (±0.01 V)	J_{SC} (mA/cm^2)	FF (±0.01)	η_p (%)	J_s (mA/cm^2)	*n*	R_s (Ω·cm^2)	R_p (10 ^{6}Ω·cm^2)
DPASQ	1.0	5.5(±0.1)	0.73	4.0(±0.1)	9.3×10^{-11}	1.56	3.8	116
DPSQ	0.91	7.2(±0.1)	0.70	4.8(±0.2)	8.6×10^{-9}	1.77	1.7	1.5
PSQ	0.68	9.5(±0.1)	0.69	4.6 (±0.2)	1.6×10^{-7}	1.46	3.6	48.9
1-NPSQ	0.90	6.9(±0.1)	0.71	4.3(±0.1)	5.4×10^{-8}	1.84	9.3	1.59
SQ	0.79	8.0(±0.1)	0.68	4.4 (±0.1)	5.9×10^{-8}	1.66	4.7	45.3
ASSQ	0.92	6.3(±0.1)	0.63	3.7(±0.1)	2.5×10^{-9}	1.64	41.2	27.1

with its broadened absorption band in the visible and NIR, the PSQ/C_{60} cells have J_{sc} = 9.5 ± 0.1 mA/cm^2, as indicated in Table 2.

The selected area diffraction (SAED) patterns for as-cast squaraine donors other than PSQ are featureless, indicative of an amorphous morphology (Figure 6a). The clusters in the annealed DPSQ films suggest a single crystal structure with diffraction features of the SAED pattern indexed to the (010) and (30$\bar{1}$) crystal planes (Figure 6b). The annealed 1-NPSQ and SQ films are also polycrystalline (see Figure 6c and f, respectively). The formation of PSQ nanocrystallites both before and after thermal annealing is apparent in Figure 6d and e. While the diffraction patterns show defined spots, their intensity is relatively weak and distributed in Debye–Scherrer ring patterns that are indexed to the (100) and (010) crystal reflections. In general, thermal annealing of amorphous, symmetric squaraines results in the formation of nanocrystallites, whereas the asymmetric DPASQ and ASSQ films are amorphous.

Figure 7 shows a correlation between OPV FF at 1 sun and thin film density. With the increase in density from 1.27 ± 0.02 g/cm^3 for ASSQ to 1.45 ± 0.05 g/cm^3 for DPASQ thin films, we observe a corresponding increase in FF from 0.63 ± 0.01 to 0.73 ± 0.01, suggesting that compact molecular stacking improves the charge transport and collection. Moreover, the densities of the DPSQ and SQ thin films are consistent with those calculated from the single-crystal structural data.[14] Here, the DPSQ density of 1.39 ± 0.04 g/cm^3 is larger than that of SQ due to the close molecular stacking resulting from the inclusion of the planar, diphenyl functional groups. As shown previously, this produces a crystal habit with close intermolecular, cofacial π-stacking and, hence, an increase in hole mobility.[14] As shown in Figure 4a, the DPSQ/C_{60} cells have higher FF compared with SQ/C_{60} cells throughout the range of measured power intensities.

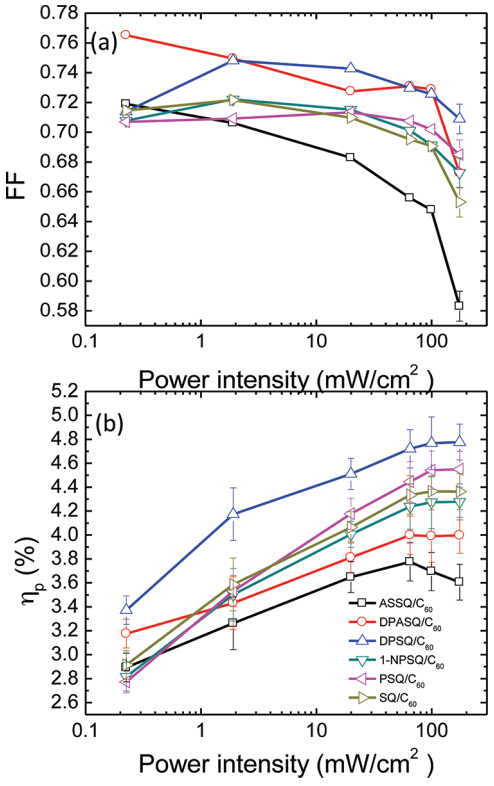

Figure 4. (a) Fill factors (FF) and (b) power conversion efficiencis (η_p) as functions of AM1.5G spectral illumination power intensities (corrected for solar spectral mismatch) of the six as-cast *f*SQ/C_{60} cells in Figure 3.

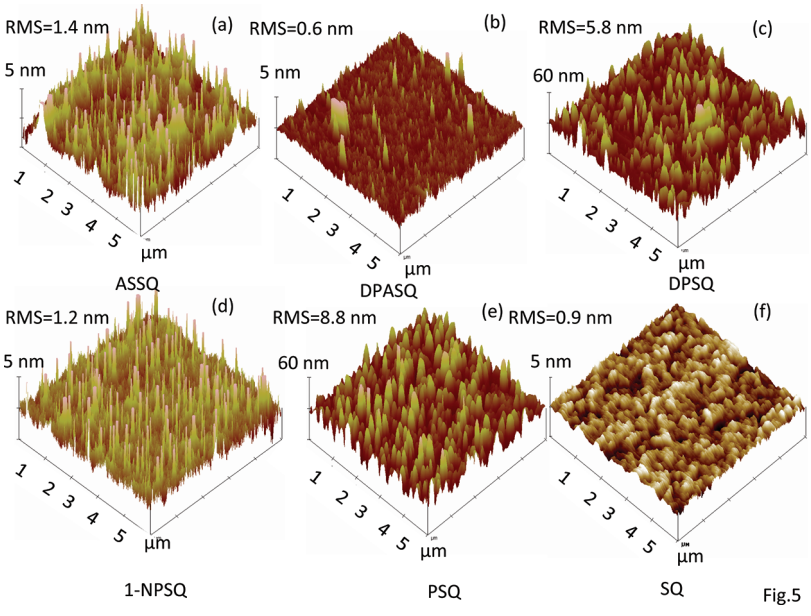

Fig.5

Figure 5. Perspective atomic force microscope (AFM) images of as-cast (a) ASSQ, (b) DPASQ, (c) DPSQ, (d) 1-NPSQ, (e) PSQ, and (f) SQ films deposited on indium tin oxide (ITO)-coated glass with a 80 Å thick surface layer of MoO_3. Here, rms is the root-mean-square roughness of the films.

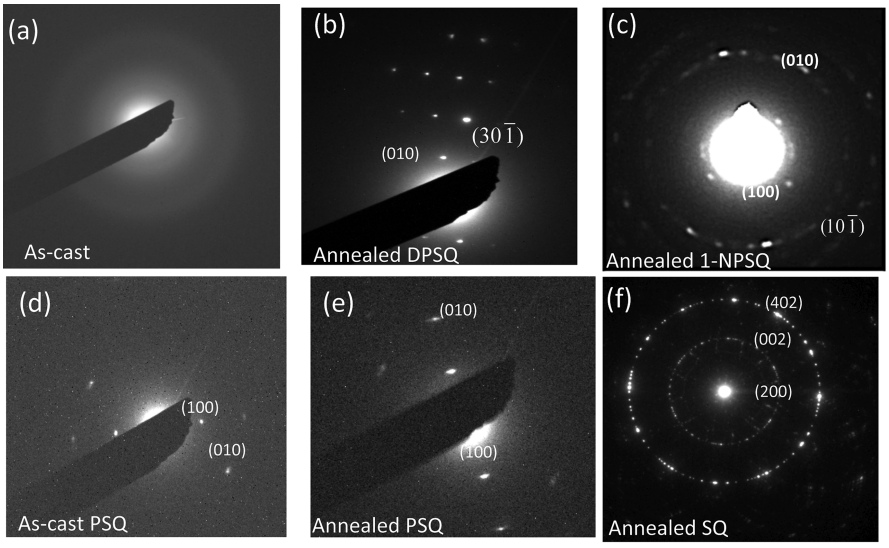

Figure 6. Selected-area electron diffraction patterns of (a) as-cast SQ; (b) annealed DPSQ; (c) annealed 1-NPSQ; (d) as-cast PSQ; (e) annealed PSQ; and (f) annealed SQ films.

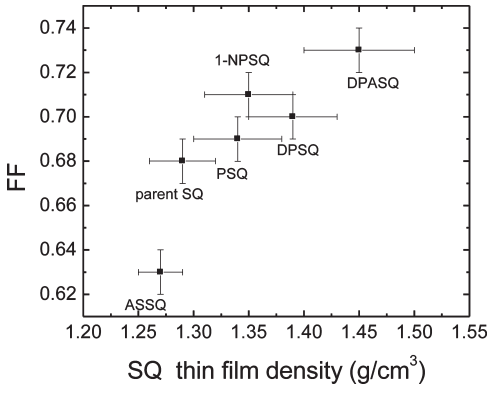

Figure 7. Fill factor (FF) *versus* the mass density of six functionalized SQs.

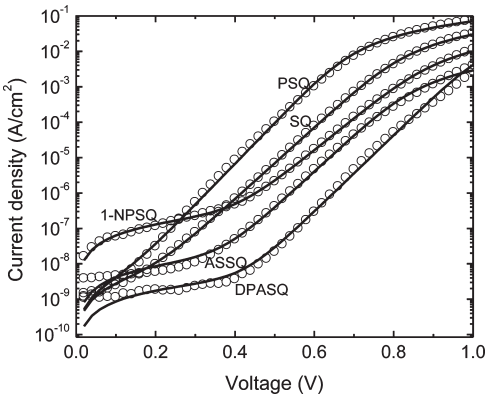

Figure 8. Dark current density *versus* voltage characteristics (open circles) of five as-cast *f*SQs/C_{60} cells in Figure 3. The solid lines are fits to the *J*−*V* characteristics based on the modified ideal diode equation.

To further understand the performance of the *f*SQ/C_{60} cells, the modified ideal diode equation for organic heterojunctions,[16,17]

$$J = J_s\left[\exp(q(V - JR_s)/nk_BT) - \frac{k_{PPd}}{k_{PPd,eq}}\right] + \frac{V_a - JR_s}{R_p}$$

is applied to fit the dark *J*−*V* characteristics. Here, J_s is the reverse saturation current density, q is the electron charge, R_s is the series resistance, n is the ideality factor, k_B is the Boltzmann constant, T is the temperature, and R_p is the parallel (or shunt) resistance. For simplicity, the ratio of the polaron pair dissociation rate to its equilibrium value is assumed to be $k_{PPd}/k_{PPd,eq} \approx 1$. As shown in Table 2, ASSQ-based cells have the largest series resistance ($R_s = 41.2 \pm 4.6\ \Omega\cdot cm^2$) along with the lowest molecular density of 1.27 ± 0.02 g/cm^3. Their high resistance results in a sharp roll-off in FF with power intensity, as shown in Figure 4a. In contrast, DPASQ, with four phenyl groups on each molecule as shown in Figure 1, has intimate molecular π-stacking and the highest density. As a consequence, DPASQ/C_{60} cells have R_s that is one order of magnitude lower than ASSQ/C_{60} cells (Table 2 and Figure 8).

Polycrystalline PSQ introduces a rough interface with C_{60}, resulting in high exciton dissociation efficiency. On the other hand, increased roughness allows the C_{60} to directly contact the anode, resulting in a thousand-fold increase in J_s in comparison with cells based on DPASQ/C_{60} (Table 2 and Figure 8). The high J_s leads to a reduction in V_{oc} = 0.68 V, which limits the device efficiency to 4.6 ± 0.2%.

The exciton diffusion length is an important parameter to consider in the design of solar cells. Typically, L_D is limited due to weak intermolecular interactions. Thermal annealing is, therefore, necessary to generate a distribution of crystallites whose dimension is ~L_D to promote exciton diffusion to a nearby donor−acceptor interface, and thus efficient dissociation. The parent SQ has a relatively short L_D (1.6 ± 0.2 nm), resulting in an optimum SQ donor thickness of only ~65 Å.[10,21]

TABLE 3. Performance of Annealed *f*SQ/C_{60} Solar Cells under 1 sun, AM1.5G Simulated Illumination

molecular species	annealing temp (°C)	V_{oc} (±0.01 V)	J_{SC} (mA/cm^2)	FF(±0.01) P_0 = 1 sun[a]	η_p (%) at P_0 = 1 sun
DPASQ	70	0.98	6.25(±0.15)	0.72	4.4(±0.2)
DPSQ	80	0.94	7.40(±0.14)	0.72	5.2(±0.2)
1-NPSQ	70	0.91	6.97(±0.14)	0.71	4.5(±0.2)
SQ	90	0.73	9.27(±0.22)	0.68	4.6(±0.1)
ASSQ	70	0.90	6.20(±0.11)	0.63	3.6(±0.1)

[a] P_0 is the incident power. One sun = 100 mW/cm^2 at AM1.5G spectral illumination.

TABLE 4. Power Conversion Efficiency (η_p) at 1 sun Illumination Obtained from Optimized *f*SQ/C_{60} Solar Cells

device	$\eta_{p(max)}$ (%)
DPASQ/C_{60}	4.4 ± 0.2
DPSQ/C_{60}	5.2 ± 0.2
PSQ/C_{60}	4.6 ± 0.2
1-NPSQ/C_{60}	5.7 ± 0.6
SQ/C_{60}	4.6 ± 0.1
ASSQ/C_{60}	3.6 ± 0.1

As shown in Table 1, the asymmetric *f*SQs have significantly longer diffusion lengths with L_D = 10.7 ± 0.2 nm for DPASQ and 11.0 ± 0.6 nm for ASSQ. However, their photon absorption in the green limits the photocurrent generated in such cells. The symmetric NIR absorptive DPSQ and 1-NPSQ have L_D approximately double than that of SQ. Thus, the optimum thickness of 1-NPSQ is 200 Å.[15]

Thermal annealing has been proven to be effective in creating squaraine nanocrystalline structures[10] that lead to higher efficiency OPVs. This strategy has been applied to the six *f*SQ/C_{60} devices with the same donor thicknesses of 85 ± 5 Å. As shown in Table 2 (as-cast devices) and Table 3 (annealed devices), annealing improves the efficiencies of all symmetric *f*SQ-based cells. In particular, DPSQ/C_{60} cell efficiency is increased from 4.8 ± 0.2% (as-cast) to 5.2 ± 0.2% (80 °C). In contrast, the ASSQ/C_{60}-based cells have a reduced efficiency following thermal annealing. Furthermore, annealing PSQ results in roughening and, hence, the formation of shorts. The optimized 1-NPSQ/C_{60} cells (Table 4) have the highest efficiency of 5.7 ± 0.6% at 1 sun illumination.

Finally, the relatively high FF (0.73 ± 0.01) of the DPASQ/C_{60} cell results from its compact molecular stacking, allowing for low resistance to charge transport and ultimately efficient hole collection at the anode. The PSQ/C_{60} cells with efficiency of 4.6 ± 0.2% are only slightly inferior to the DPSQ/C_{60} cells, resulting from its tendency to form crystalline structures whose dimensions are on the order of L_D.

CONCLUSIONS

A family of functionalized squaraine molecules has been synthesized with molecular structures intended to improve intermolecular $\pi-\pi$ stacking. This strategy has led to improved exciton diffusion lengths and conductivities over the parent squaraine lacking the planar end group motif. Solar cells employing an asymmetric molecule with diphenyl end groups (DPASQ) have a FF = 0.73 ± 0.01 and V_{oc} = 1.0 V, although its absorption in the green ultimately limits the increase in J_{sc}. We find a correlation between solar cell FF with the *f*SQ thin film density, providing support for the molecular design concept that planar end groups result in close intermolecular stacking and, hence, improved charge transport and exciton diffusion. Finally, thermal annealing of the films results in the formation of nanocrystalline morphologies that lead to further improvements in device performance.

EXPERIMENTAL SECTION

Solar cells were grown with the following structure: indium tin oxide (ITO)/MoO_3 (80 Å)/squaraine (85 ± 5 Å)/C_{60}(400 Å)/3,4,9,10-perylenetetracarboxylic bisbenzimidazole (PTCBI) (80 Å)/Ag (1000 Å). An 80 Å thick layer of MoO_3 is thermally evaporated onto precleaned, 150 nm thick indium tin oxide (ITO)-coated glass substrates in a vacuum system with a base pressure of 10^{-7} Torr (ITO sheet resistance = 20 Ω/cm^2). The squaraine thin films were spin-coated from 1 mg/mL chloroform solutions on the MoO_3 and ITO-coated glass substrates. After spin-coating at a rate of 3000 rpm for 30 s, C_{60}, PTCBI, and the Ag cathode were sequentially thermally deposited in high vacuum. The Ag cathode was patterned by deposition through a shadow mask with an array of 1 mm diameter circular apertures.

The current density−voltage ($J-V$) characteristics and η_p of the solar cells were measured using a solar simulator with AM1.5G filters and an NREL-calibrated Si detector. Solar spectral mismatch corrections were determined using standard methods.[18] The external quantum efficiency was measured using a monochromator in combination with a Xe lamp.

The ionization energies (*i.e.*, the HOMO energies) for the *f*SQ thin films were measured by ultraviolet photoemission spectroscopy (UPS) using 21.22 eV He−I emission in a Thermo VG Scientific Clam4MCD analyzer system. Samples were prepared by thermal evaporation of a 30 nm thick Au film onto a p-type Si substrate, followed by spin-casting of the squaraines as above. Transfers between the deposition and analysis chambers were performed at <10^{-8} Torr, and the pressure in the UPS measurement chamber was <10^{-9} Torr. The analyzer resolution was ~0.15 eV, as determined by a fit to the Fermi level of Au. The lowest unoccupied molecular orbital (LUMO) energies were determined by measuring the positions of the low-energy optical absorption tails and adding those values to their HOMO energies.

To determine the *f*SQ thin film density,[19] the peak absorptions of films cast onto Si substrates from solutions with known

squaraine concentrations were measured by assuming a linear dependence of absorbance on concentration (*i.e.*, the Beer–Lambert law). The thicknesses of the *f*SQ films were determined using a variable angle and wavelength ellipsometer. Then the squaraine films were dissolved in 6 mL of chloroform for 5 min, and the absorption of the *f*SQ solutions was measured. Finally, the densities of *f*SQ films were calculated using a least-squares fit to the dependence of concentration in solution (as determined from the absolute absorption) on the measured film volume.[19]

The exciton diffusion length was measured using spectrally resolved photoluminescent quenching adapted for optically thin films.[20,21] Samples were deposited in pairs on Si substrates, with one sample capped with an exciton blocking layer of bathocuproine and the other with a C_{60} exciton quenching layer. The photoluminescence excitation spectra of the samples were measured in a PTI QuantaMaster spectrofluorometer at an incidence angle of 30°.

Samples for atomic force microscopy operated in the tapping mode were prepared by casting the squaraine thin films on 80 Å thick MoO_3 films predeposited on ITO-coated glass substrates. Selected area diffraction patterns were obtained using a JEOL 2010F transmission electron microscope, where samples were prepared via wet-transfer of cast and thermally annealed squaraine films onto Cu grids coated with carbon type-B.

Acknowledgment. This work was supported in part by the Center for Solar and Thermal Energy Conversion at the University of Michigan (Award No. DE-SC00000957; S.R.F., analysis, G.W., experiment and analysis, X.X., experiment), the Air Force Office of Scientific Research (K.J.B.), the Department of Energy Frontier Center at the University of Southern California (award DE-SC0001011, S.W. and M.E.T.), and Global Photonic Energy Corp. (K.J.B., diffusion lengths). We thank C. Kyle Renshaw for assistance with UPS measurement and Lincoln Hall and Vyacheslav V. Diev for assistance with molecular design and synthesis.

REFERENCES AND NOTES

1. Hoven, C. V.; Dang, X. D.; Coffin, R. C.; Peet, J.; Nguyen, T. Q.; Bazan, G. C. Improved Performance of Polymer Bulk Heterojunction Solar Cells through the Reduction of Phase Separation via Solvent Additives. *Adv. Mater.* **2010**, *22*, 63–66.
2. Kim, M. S.; Kim, B. G.; Kim, J. Effective Variables to Control the Fill Factor of Organic Photovoltaic Cells. *ACS Appl. Mater. Interfaces* **2009**, *1*, 1264–1269.
3. Chen, H. Y.; Hou, J. H.; Zhang, S. Q.; Liang, Y. Y.; Yang, G. W.; Yang, Y.; Yu, L. P.; Wu, Y.; Li, G. Polymer Solar Cells with Enhanced Open-Circuit Voltage and Efficiency. *Nat. Photonics* **2009**, *3*, 649–653.
4. Peumans, P.; Uchida, S.; Forrest, S. R. Bulk Heterojunction Photovoltaic Cells Using Small-Molecular-Weight Organic Thin Films. *Nature* **2003**, *425*, 158–162.
5. Yang, F.; Sun, K.; Forrest, S. R. Efficient Solar Cells Using All-Organic Nanocrystalline Networks. *Adv. Mater.* **2007**, *19*, 4166–4171.
6. Wei, G. D.; Wang, S. Y.; Renshaw, K.; Thompson, M. E.; Forrest, S. R. Solution-Processed Squaraine Bulk Heterojunction Photovoltaic Cells. *ACS Nano* **2010**, *4*, 1927–1934.
7. Silvestri, F.; Irwin, M. D.; Beverina, L.; Facchetti, A.; Pagani, G. A.; Marks, T. J. Efficient Squaraine-Based Solution Processable Bulk-Heterojunction Solar Cells. *J. Am. Chem. Soc.* **2008**, *130*, 17640–17641.
8. Bagnis, D.; Beverina, L.; Huang, H.; Silvestri, F.; Yao, Y.; Yan, H.; Pagani, G. A.; Marks, T. J.; Facchetti, A. Marked Alkyl- vs Alkenyl-Substitutent Effects on Squaraine Dye Solid-StateStructure, Carrier Mobility, and Bulk-Heterojunction Solar Cell Efficiency. *J. Am. Chem. Soc.* **2010**, *132*, 4074–4075.
9. Wei, G. D.; Wang, S. Y.; Sun, K.; Thompson, M. E.; Forrest, S. R. Solvent Annealed Crystalline Squaraine: $PC_{70}BM$ (1:6) Solar Cells. *Adv. Energ. Mater.* **2011**, *1*), 184–187.
10. Wei, G. D.; Lunt, R. R.; Sun, K.; Wang, S. Y.; Thompson, M. E.; Forrest, S. R. Efficient, Ordered Bulk Heterojunction Nanocrystalline Solar Cells by Annealing of Ultrathin Squaraine Thin Films. *Nano Lett.* **2010**, *10*, 3555–3559.
11. Walker, B.; Tamayo, A. B.; Dang, X. D.; Zalar, P.; Seo, J. H.; Garcia, A.; Tantiwiwat, M.; Nguyen, T. Q. Nanoscale Phase Separation and High Photovoltaic Efficiency in Solution-Processed, Small-Molecule Bulk Heterojunction Solar Cells. *Adv. Funct. Mater.* **2009**, *19*, 3063–3069.
12. Sreejith, S.; Carol, P.; Chithra, P.; Ajayaghosh, A.; Squaraine Dyes, A. Mine of Molecular Materials. *J. Mater. Chem.* **2008**, *18*, 264–274.
13. Mayerhoffer, U.; Deing, K.; Gruß, K.; Braunschweig, H.; Meerholz, K.; Wurthner, F. Outstanding Short-Circuit Currents in BHJ Solar Cells Based on NIR-Absorbing Acceptor-Substituted Squaraines. *Angew. Chem., Int. Ed.* **2009**, *48*, 8776–8779.
14. Wang, S. Y.; Hall, L.; Diev, V. V.; Wei, G. D.; Xiao, X.; Djurovich, P. I.; Forrest, S. R.; Thompson, M. E. N,N-Diarylanilinosquaraines and Their Application to Organic Photovoltaics. *Chem. Mater.* **2011**, *23*, 4789–4798.
15. Wei, G. D.; Xiao, X.; Wang, S. Y.; Sun, K.; Zimmerman, J. D.; Thompson, M. E.; Forrest, S. R. Arylamine-Based Squaraine Donor for Use in Organic Solar Cells. *Nano Lett.* **2011**, *11*), 4261–4264.
16. Rand, B. P.; Burk, D. P.; Forrest, S. R. Offset Energies at Organic Semiconductor Heterojunctions and Their Influence on the Open-Circuit Voltage of Thin-Film Solar Cells. *Phys. Rev. B* **2007**, *75*), 115327.
17. Giebink, N. C.; Wiederrecht, G. P.; Wasielewski, M. R.; Forrest, S. R. Ideal Diode Equation for Organic Heterojunctions. I. Derivation and Application. *Phys. Rev. B* **2010**, *82*, 155305.
18. Shrotriya, V.; Li, G.; Yao, Y.; Morarty, T.; Emery, K.; Yang, Y. Accurate Measurement and Characterization of Organic Solar Cells. *Adv. Funct. Mater.* **2006**, *16*, 2016–2023.
19. Xiang, H. F.; Xu, Z. X.; Roy, V. A. L.; Che, C. M.; Lai, P. T. Method for Measurement of the Density of Thin Films of Small Organic Molecules. *Rev. Sci. Instrum.* **2007**, *78*, 034104.
20. Lunt, R. R.; Giebink, N. C.; Belak, A. A.; Benziger, J. B.; Forrest, S. R. Exciton Diffusion Lengths of Organic Semiconductor Thin Films Measured by Spectrally Resolved Photoluminescence Quenching. *J. Appl. Phys.* **2009**, *105*, 053711.
21. Bergemann, K. J.; Forrest, S. R. Measurement of Exciton Diffusion Lengths in Optically Thin Organic Films. *Appl. Phys. Lett.* **2011**, *99*, 243303.